Torque ripple reduction in BLDC motor based on a PWM technique for open-end winding

MARCIN BASZYNSKI

AGH – University of Science and Technology
Poland
e-mail: mbaszyn@agh.edu.pl

Abstract: The article presents a modulation method for BLDC motors with unconnected windings. This method uses two full bridges (or three 12-switch H-bridges). The use of the described modulation enables reducing the motor current variable and increasing (fourfold in relation to the switching frequency) the motor current ripple frequency. The most important benefit of using a 12-switch inverter is the twofold reduction of the dc-link voltage while maintaining the rated rpm (voltage reduction in comparison to a typical supply method). A voltage reduction causes a reduction in losses on semi-conductor elements. The article also demonstrates that the proposed modulation technique significantly shortens the time of current commutation between windings.

Key words: BLDC motor, open-end winding, PWM technique, unipolar modulation

1. Introduction

In recent years, owing to the developments in power electronics and the availability of cheap semiconductor components, numerous research centers started work on stepper, induction and reluctance brushless motors [1] or PMSM permanent magnet motors and BLDC motors [2–4]. Thanks to easy control methods and high power density, this last type has found a number of applications in various sectors of industry: automotive [5, 6], automation, etc. Even though BLDC motors have been known for years, there are still numerous research projects aiming to improve their performance. One of the main areas of the research are sensorless methods [5–9] based on back electromotive force (BEMF) measurements in a non-energized winding, as well as modifications to pulse width modulation (PWM) allowing for the detection of the rotor position at start-up (BEMF near zero). Additional impulses causing current flow in subsequent windings

are interwoven into the PWM cycles [9, 10]. Based on observations of the rate at which the current increases, the inductivity of the circuit is determined, thus showing the position of the rotor relative to the stator. Compared to the standard modulation, extra pulses are shorter by not bringing significant moments of parasitic and do not affect the motor.

Another important aspect of research on BLDC motors is the Commutation Torque Ripple due to the loss of control over the current during current switching between consecutive windings, as well as the non-zero inductance of the winding that starts the conduction, which limits the rate of current increase. One concept meant to minimize the torque ripple during commutation involves special modulation techniques that allow the simultaneous flow of current through all the motor windings [3, 11–13].

Motor braking requires the receipt of energy from the rotating mass of the rotor and dampening it in the resistors, transferring it to the energy storage or returning it to the supply network [14–16]. The phenomenon of energy storage in a rotating mass can be used to improve the quality of electricity [17].

An important research area is related to methods of rotational speed regulation. The change of the rotational speed is performed by changing the average the value of voltage applied to motor windings. The following techniques can be used for this purpose: Pulse Width Modulation (PWM) [8, 10], Pulse Amplitude Modulation (PAM) [8, 10], and Hysteresis current control [1]. The first of the mentioned methods requires maintaining a constant voltage at the dc-link capacitor, and the regulation of the voltage at motor terminals is performed by changing the duty cycle of power inverter pulses. In the PAM method, the voltage at the dc-link capacitor is subject to regulation (depending on rotational speed), and the power inverter transistors are conducting current for $2/3\pi$ (their switching frequency results from rotational speed). The capacitor voltage can be regulated using e.g. a thyristor rectifier [8]. Analyzing the properties of both methods, it can be concluded that PWM power inverters are used for low-speed motors, while PAM power inverters are better suited for devices with motors of high rotational speed [8].

A BLDC motor can include delta winding connections powered from six transistor inverters [18–22]. In such a connection, current always flows through three windings (in a delta winding connection, the current flows through two phases). When maintaining a constant electromagnetic moment, this causes the phase currents and ripples to have higher values in a delta connection than in a star connection. In the presented solution the ripples are reduced, the dc-link voltage is reduced twofold and the dc-link current frequency is increased fourfold.

Halving the dc-link voltage reduces the losses during transistor switching operations (in comparison to classic BLDC motor supply methods [20–24]).

2. Open-end winding PWM technique

Typically, three-phase BLDC motors are connected in star configuration, even if the beginnings and ends of windings are available. Due to the method of feeding, motors of this type cannot be connected in delta configuration [11–20].

The BEMF of a BLDC motor is described by the relationship:

$$e = k \cdot \omega, \tag{1}$$

where: e is the motor BEMF voltage, k is the excitation coefficient, ω is the rotor angular speed.

When motor windings are connected in star configuration, the instantaneous voltage at a single winding is equal to half of the DC link voltage. This means that the DC link voltage must be at least twice as high as implied by Equation (1) in order to achieve the required rotational speed. A surplus of the DC link voltage above the BEMF is required in order to force a current flow in the windings. In the case of open-end winding motors it is possible to supply a motor by two bridge power inverters connected respectively to the beginnings and ends of windings (Fig. 1).
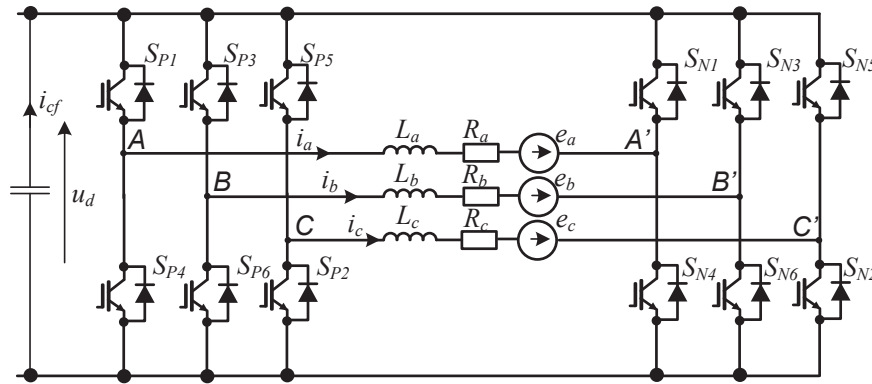

Fig. 1. Open-end winding BLDC motor power supply scheme

The DC link voltage (u_d) is connected directly to every winding, therefore a voltage not lower than the BEMF is sufficient for achieving the required speed. This means that the DC link voltage of the system from Fig. 1, necessary for achieving the required speed, is approx. two times lower than for a system with the winding connected in star configuration. Therefore, the system from Fig. 1 can be realized using less expensive elements, transistors of lower permissible EC voltage, less expensive transistor drivers, and capacitors of lower operating voltage. The ability to use less expensive elements compensates for the need to use an additional semiconductor bridge. Moreover, each of the windings is supplied from a separate power inverter branch, therefore there is no problem with current switching between windings when the rotor passes the switching points. A lower voltage at the dc-link capacitor results also in lower losses at semiconductor elements.

With windings connected as in Fig. 1 it is possible to use unipolar modulation analogous to the modulation used in one-phase systems, which makes it possible to obtain a frequency of the ac component of the current that is two times higher than the transistor switching frequency. This part of the proposed solution makes it possible to use motor chokes (low-pass filters) of inductance that is two times lower than in the conventional solution, while keeping the same value of the ac component of the current. The idea of this modulation is presented in Fig. 2.

If the instantaneous value of the signal u_{ref} is positive and greater than that of the saw-tooth waveform, the upper transistor of the branch S_{P1} is switched on, which makes the potential of the beginning of the winding equal to the potential of the positive electrode of the dc-link capacitor. From this it follows that the voltage at the beginning of the winding (point A) measured with relation to point M (Fig. 3) is equal to the power supply voltage U_d.

The torque in a BLDC motor is proportional to the current, therefore the torque pulsation of a motor supplied in the described way is characterized by a very high frequency, four times higher than the switching frequency and a relatively low value of pulsation. The four times greater value of the frequency of the ac component with relation to the transistor switching frequency is obtained thanks to the phase shift of the saw-tooth waveforms in the PWM signal generator.

As shown in Fig. 2, one period of transistor operation consists of four stages resulting from the conducting semiconductor elements. All operating states and the path of current flow in the circuit are presented in Fig. 4. The current flow path has been marked in black, and the elements which do not take part in the current flow are marked in grey.

A precise analysis of the operating states of transistors during one switching cycle reveals that the period consists of four stages, however, the first and third stage are identical. In the first stage of the cycle (Fig. 4(a)) current flows through transistors S_{P1} and S_{N4} and it is forced by the difference between the dc-link voltage U_d and the BEMF of phase a (e_a). After switching off the transistor S_{N4} and applying a gating impulse to transistor S_{N1}, under the influence of the energy
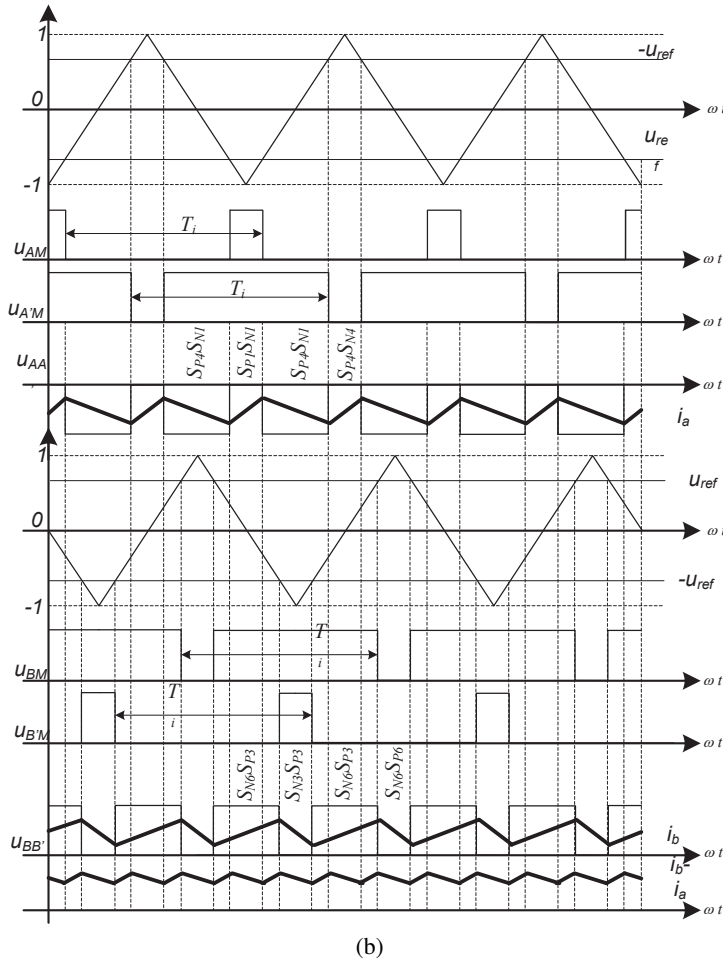

(a)

(b)
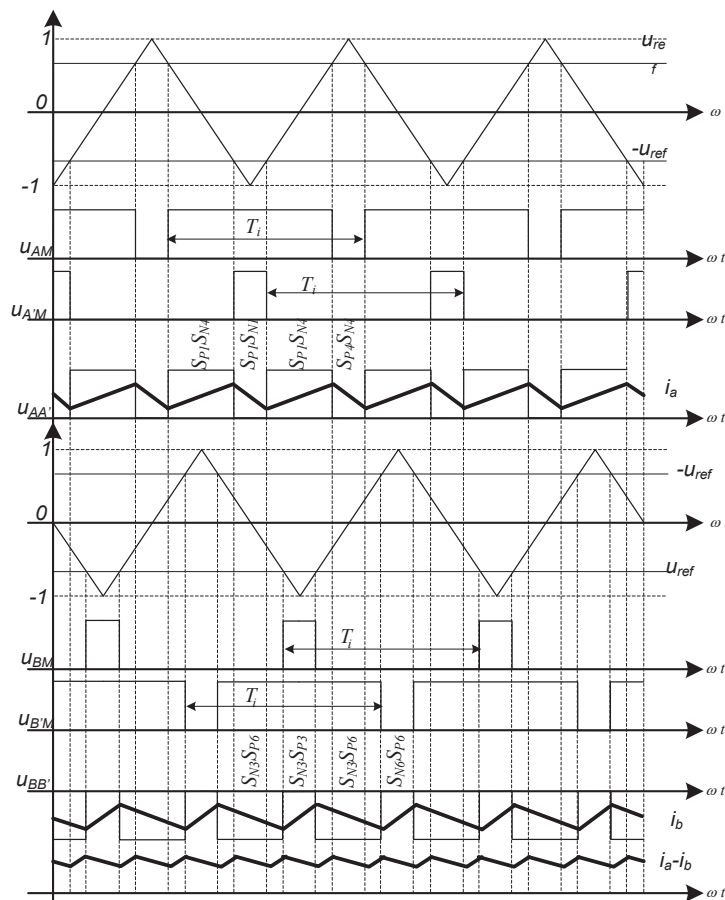
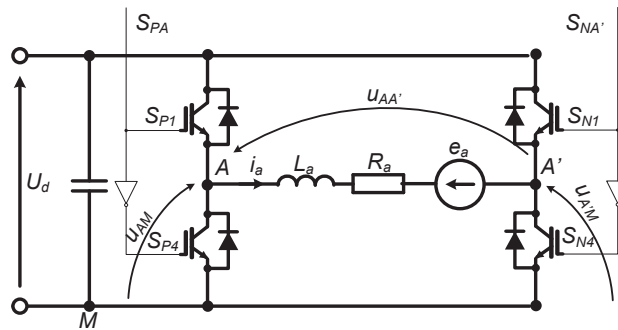Fig. 2. Method for generating the PWM signal for current flow: (a) from point A to A′ and from B′ to B; (b) from point A′ to A and from B to B′
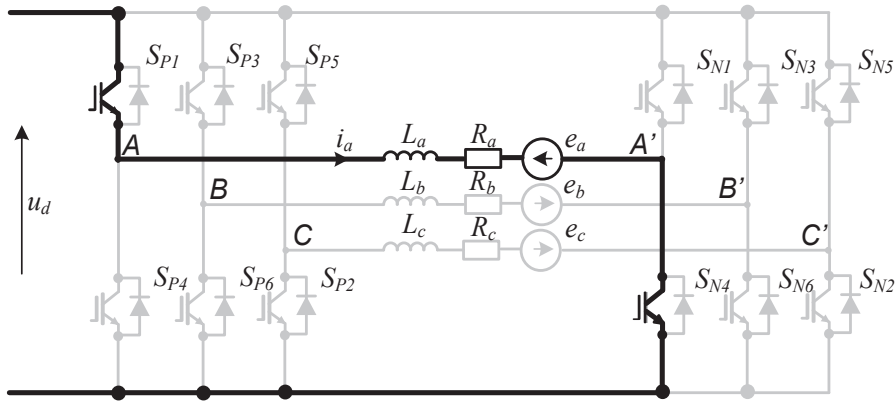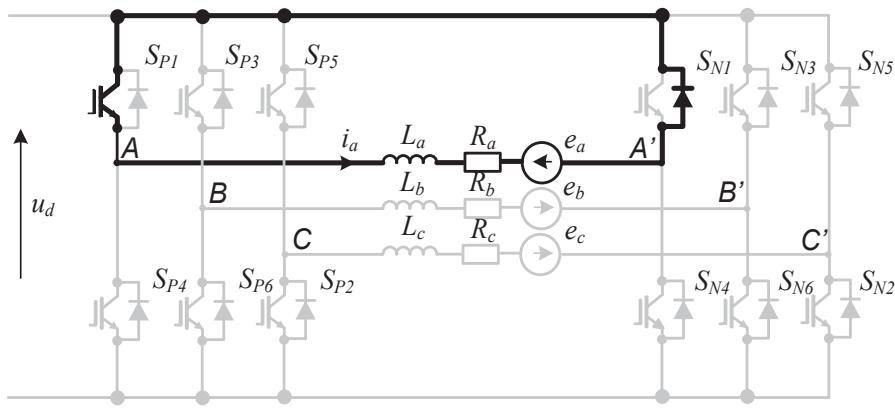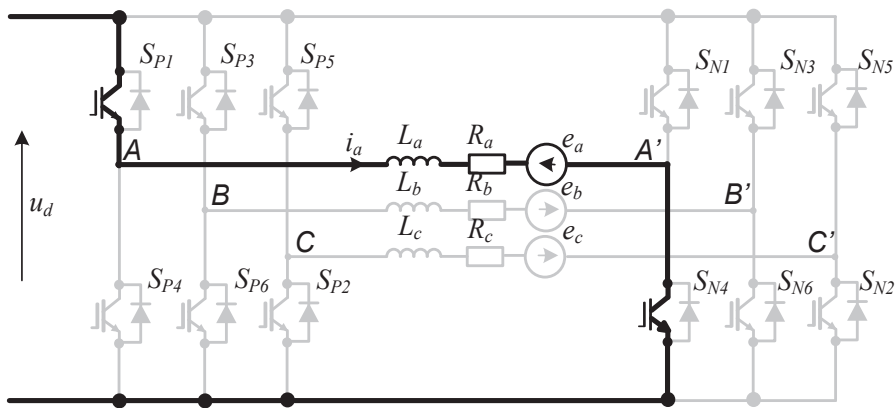

Fig. 3. Marking of the voltages for one phase of the motor
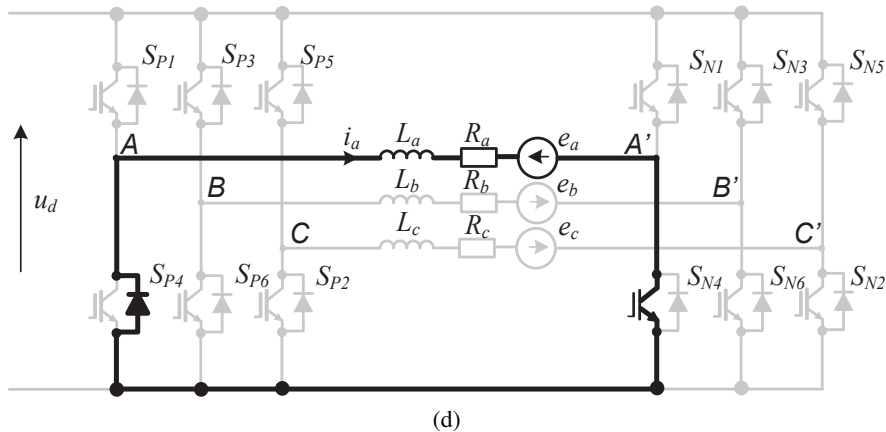
(a)

(b)

(c)

(d)

Fig. 4. Path of current flow during one switching period

accumulated in the inductance of the windings and the BEMF, current flows through the diode of transistor S_{N1}, transistor S_{N1} is not conducting current, Fig. 4(b).

In this state there is no exchange of energy between the dc-link capacitor and the motor. The following stage of modulation is identical with the first one, current flows through transistors S_{P1} and S_{N4}. In the last stage of modulation, after opening transistor S_{P1} and driving transistor S_{P4}, current flows through transistor S_{N4} and the diode antiparallel to transistor S_{P4}. Like in the case indicated in Fig. 4(b), current flows under the influence of energy accumulated in the magnetic field of the inductance of the windings and the BEMF. In a BLDC motor, current flows through two windings simultaneously, however, Fig. 4 presents the current path for one of the phases only, because a similar analysis can be performed for the remaining windings.

3. PWM generator

At any given time, current in three-phase BLDC motors flows through two windings, and the third one remains unpowered. Therefore, there are three different combinations of conducting phases. Taking into account the directions of current flow through the windings, a total of six different operational states of the windings can be obtained. As it results from Fig. 2, the saw-tooth waveforms of the PWM generator for the conducting phases are shifted with respect to each other by $n/2$. In order to ensure proper modulation for all combinations of conducting phases, it is necessary to generate two saw-tooth waveforms shifted with respect to each other, and to use them sequentially, in accordance with the sequence of powered phases that results from the direction of the motor rotation. Fig. 5 presents an example of an assignment of the carrier waveforms (*carrier A*, and *carrier B* shifted by $\pi/2$) to the conducting phases.

In order to illustrate better the assignment of the carrier waveforms to the powered windings, signals from the sensors of rotor position (H_A, H_B, H_C) and BEMF (e_A, e_B, e_C) have also been included in Fig. 5.
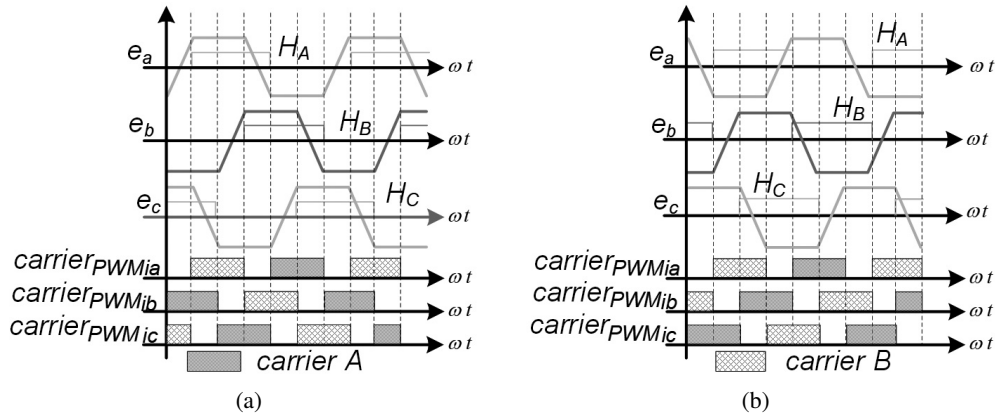
Fig. 5. Assignment of the carrier waveforms to the conducting phases

As it results from Fig. 5, the assignment can be made on the basis of signals from the rotor position sensor. Moreover, in the combination proposed in Fig. 5 the direction of rotation does not affect the assignment of the carrier waveforms to the respective phases.

The following assignment functions can be assumed on the basis of Fig. 5:

$$carrier_{\text{PWM}_{ia}} = \begin{cases} carrier_B & \text{if } \left(H_A \wedge \overline{H_B}\right) \\ carrier_A & \text{if } \left(H_B \wedge \overline{H_A}\right) \end{cases}$$

$$carrier_{\text{PWM}_{ib}} = \begin{cases} carrier_B & \text{if } \left(H_B \wedge \overline{H_C}\right) \\ carrier_A & \text{if } \left(H_C \wedge \overline{H_B}\right) \end{cases} , \qquad (2)$$

$$carrier_{\text{PWM}_{ic}} = \begin{cases} carrier_B & \text{if } \left(H_C \wedge \overline{H_A}\right) \\ carrier_A & \text{if } \left(H_A \wedge \overline{H_C}\right) \end{cases}$$

where: $carrier_{\text{PWM}_{ia}}$ is the saw-tooth (carrier) waveform used by the PWM generator for motor phase a, $carrier_{\text{PWM}_{ib}}$ is the saw-tooth (carrier) waveform used by the PWM generator for motor phase b, $carrier_{\text{PWM}_{ic}}$ is the saw-tooth (carrier) waveform used by the PWM generator for motor phase c.

4. Switching logic

Information about the position of the rotor with respect to the windings is necessary in order to properly supply a BLDC motor. Determination of the rotor position with respect to the stator is realized using Hall sensors or sensorless methods. The control system supplies adequate windings with power on the basis of the rotor position information. Waveforms of BEMF, signals from the sensors of rotor position (H_A, H_B, H_C), and transistor control pulses are presented in Fig. 6. The figure has been prepared for motoring operation and for both directions of rotation.
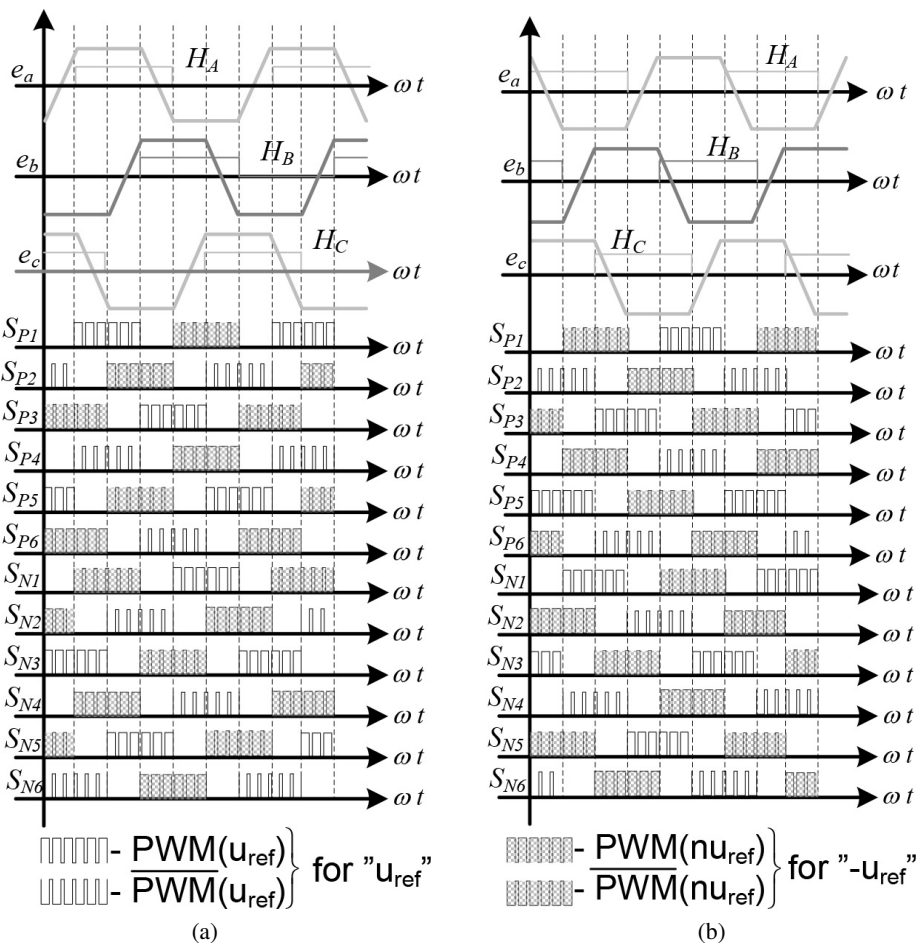
Fig. 6. Waveforms of BEMF, rotor position signals, and transistor control pulses for both directions of rotation: (a) clockwise CW and (b) counterclockwise CCW

Logic functions for easy implementation of control have been determined on the basis of Fig. 6. Two waveforms have been used for transistor control: $\text{PWM}_{u\,\text{ref}}$ obtained from comparing the saw-tooth waveform with the reference signal u_{ref}, and $\text{PWM}_{nu\,\text{ref}}$ which uses the signal u_{ref} for comparison.

The control functions for both directions only differ in the method of assigning the signals $\text{PWM}_{u\,\text{ref}}$ and $\text{PWM}_{nu\,\text{ref}}$. After introducing the relationship:

$$\text{PWM}_1 = \begin{cases} \text{PWM}_{u\,\text{ref}} & \text{if CW} \\ \text{PWM}_{nu\,\text{ref}} & \text{if CCW} \end{cases}$$

$$\text{PWM}_2 = \begin{cases} \text{PWM}_{nu\,\text{ref}} & \text{if CW} \\ \text{PWM}_{u\,\text{ref}} & \text{if CCW} \end{cases} \qquad . \qquad (3)$$

Finally the switching logic functions:

$$
\begin{aligned}
S_{P1} &= \left(H_A \wedge \overline{H}_B \wedge \mathrm{PWM}_1\right) \vee \left(\overline{H}_A \wedge H_B \wedge \mathrm{PWM}_2\right) \\
S_{P2} &= \left(H_C \wedge \overline{H}_A \wedge \mathrm{PWM}_1\right) \vee \left(\overline{H}_C \wedge H_A \wedge \mathrm{PWM}_2\right) \\
S_{P3} &= \left(H_B \wedge \overline{H}_C \wedge \mathrm{PWM}_1\right) \vee \left(\overline{H}_C \wedge H_B \wedge \mathrm{PWM}_2\right) \\
S_{P4} &= \left(H_A \wedge \overline{H}_B \wedge \mathrm{PWM}_1\right) \vee \left(\overline{H}_A \wedge H_B \wedge \mathrm{PWM}_2\right) \\
S_{P5} &= \left(H_C \wedge \overline{H}_A \wedge \mathrm{PWM}_1\right) \vee \left(\overline{H}_A \wedge H_C \wedge \mathrm{PWM}_2\right) \\
S_{P6} &= \left(H_B \wedge \overline{H}_C \wedge \mathrm{PWM}_1\right) \vee \left(\overline{H}_B \wedge H_C \wedge \mathrm{PWM}_2\right) \\
S_{N1} &= \left(H_A \wedge \overline{H}_B \wedge \mathrm{PWM}_2\right) \vee \left(\overline{H}_A \wedge H_B \wedge \mathrm{PWM}_1\right) \\
S_{N2} &= \left(H_C \wedge \overline{H}_A \wedge \mathrm{PWM}_2\right) \vee \left(\overline{H}_C \wedge H_A \wedge \mathrm{PWM}_1\right) \\
S_{N3} &= \left(H_B \wedge \overline{H}_C \wedge \mathrm{PWM}_2\right) \vee \left(\overline{H}_C \wedge H_B \wedge \mathrm{PWM}_1\right) \\
S_{N4} &= \left(H_A \wedge \overline{H}_B \wedge \mathrm{PWM}_2\right) \vee \left(\overline{H}_A \wedge H_B \wedge \mathrm{PWM}_1\right) \\
S_{N5} &= \left(H_C \wedge \overline{H}_A \wedge \mathrm{PWM}_2\right) \vee \left(\overline{H}_A \wedge H_C \wedge \mathrm{PWM}_1\right) \\
S_{N6} &= \left(H_B \wedge \overline{H}_C \wedge \mathrm{PWM}_2\right) \vee \left(\overline{H}_B \wedge H_C \wedge \mathrm{PWM}_1\right)
\end{aligned}
\tag{4}
$$

Equation (4) permits transistor control independent of the direction of rotation.

5. Simulation

The verification of theoretical deliberations featured simulation testing with the use of the ICap4 programs and the Matlab/Simulink package. The ICap program was used to compare the transistor losses in the case of reducing the dc-link voltage. The Matlab package was used to conduct testing of the proposed modulation's properties.

When analyzing the distribution of transistor losses, it is necessary to separate the losses during transistor turn on, conductivity losses and losses during transistor turn off. The conductivity losses in the case of both the described topology and in a star winding connection will be identical (when using identical transistors). Due to the fact that in both types of connection, the current flowing through the windings is identical, the voltage reduction in the semi-conductor structure is the same, therefore the losses are identical. Fig. 7 and Fig. 8 present the waveforms of voltage in the transistor, transistor current, power losses and energy lost in the transistor. Fig. 7 was developed for transistor turn on, whereas Fig. 8 for transistor turn off. The analysis featured a transistor with the parameters $V_{ec} = 1200$ V, $I_c = 50$ A.

For both cases (Fig. 7, Fig. 8), the (a) figures are developed with the dc-link voltage of two times smaller than in the (b) figures.

Table 1 presents the maximum instantaneous power and lost energy values during turn on and turn off for both intermediate circuit voltages.

As shown by the data in Table 1, the total losses for a single switching period (losses on turn on and turn off, excluding conductivity losses) in the case of a transistor powered with a voltage of 400 V are 2.68 times higher than in the case of a supply of 200 V (with the same current value).
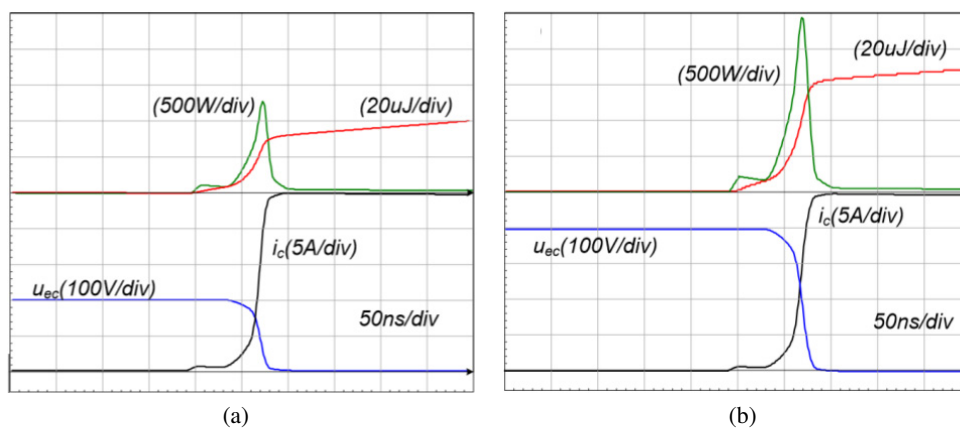
Fig. 7. Voltage waveforms in the transistor, collector and emitter, transistor current, power and energy losses:
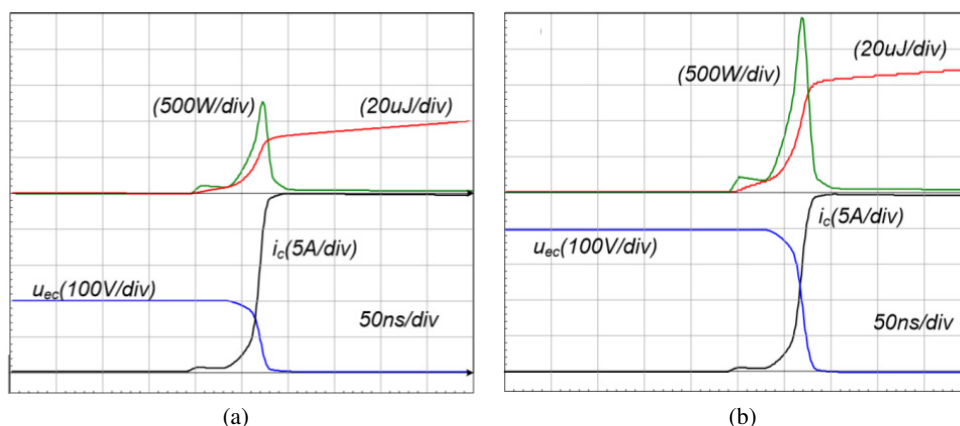(a) with a dc-link of 400 V voltage; (b) with a dc-link of 200 V voltage

Fig. 8. Voltage waveforms in the transistor, collector and emitter, transistor current, power and energy losses:
(a) with a dc-link of 400 V voltage; (b) with a dc-link of 200 V voltage

Table 1. Comparison of transistor losses at emitter- collector voltage reduction

	Turn-on 200 [V]	Turn-on 400 [V]	Turn-off 200 [V]	Turn-off 400 [V]
Power dissipation [kW]	1.19	2.55	1.1	2.3
Energy [μJ]	31.9	67.4	222	791

The described solution utilised a larger number of transistors than in classic supply methods [20–23], moreover there are more transistor switches than in a unipolar modulation [19, 20] (in a typical unipolar modulation, one of the conductive pair transistors is not switched). Simulations

using the ICap 4 program were conducted for both supply methods in order to compare the losses when switching all transistors in the tested method and in the classic unipolar technique. The simulations featured the use of the same types of transistors, an identical alternative diagram of the motor made from RLE branches. Table 2 presents the comparison of losses in both methods.

Table 2. Comparison of transistors losses at emitter- collector voltage reduction

Parameter name	Unipolar modulation 400 [V]	Presented solution 200 [V]
3 000 RPM	39.7 [J]	40.1 [J]
10 000 RPM	11.84 [J]	12.05 [J]

The BLDC motor electromagnetic torque is determined on the basis of the following relationship:

$$T_e = \frac{1}{\omega_m} \left(e_a i_a + e_b i_b + e_c i_c \right).$$

(5)

Table 3 lists the motor parameters assumed for the simulation. From Equation (5) it follows that, assuming the constancy of the back EMF only the AC component of the current causes the torque ripples. Fig. 9 presents the waveforms of the current of one of the phases, back EMF, one of the rotor position signals (Hall sensor), and electromagnetics torque (T_e). The waveforms in Fig. 9(a) were developed for the classic unipolar modulation, whereas Fig. 9(b) presents the result of the simulation for the presented solution. The same motor models, transistors and the same simulation parameters (calculation method, integration step) were used in both cases. The waveforms were recorded for the same RPM.

Table 3. List of motor parameters used in the simulation

Item	Type name	Value
1	Power	2 kW
2	Maximum speed	6 000 RPM
3	Inductance	1 mH
4	Rotor moment of inertia	$450 \cdot 10^{-3}$ kg m^2
5	Excitation coefficient	0.04 V/rad/s^{-1}
6	Winding resistance	1 Ω
7	Maximum load torque	3 Nm

As Fig. 9 shows, the AC component of the electromagnetics torque for the classic modulation is equal to 260 mNm, while for the presented solution – 169 mNm. Which means that the ripple decreases by 31.12%. The duration of the torque ripple also decreases from 624 μs (classic unipolar modulation) to 272 μs.

For the purpose of more in-depth analysis, Fig. 10 presents zoomed in current waveforms from Fig. 9. The positive waveform fragment was presented.
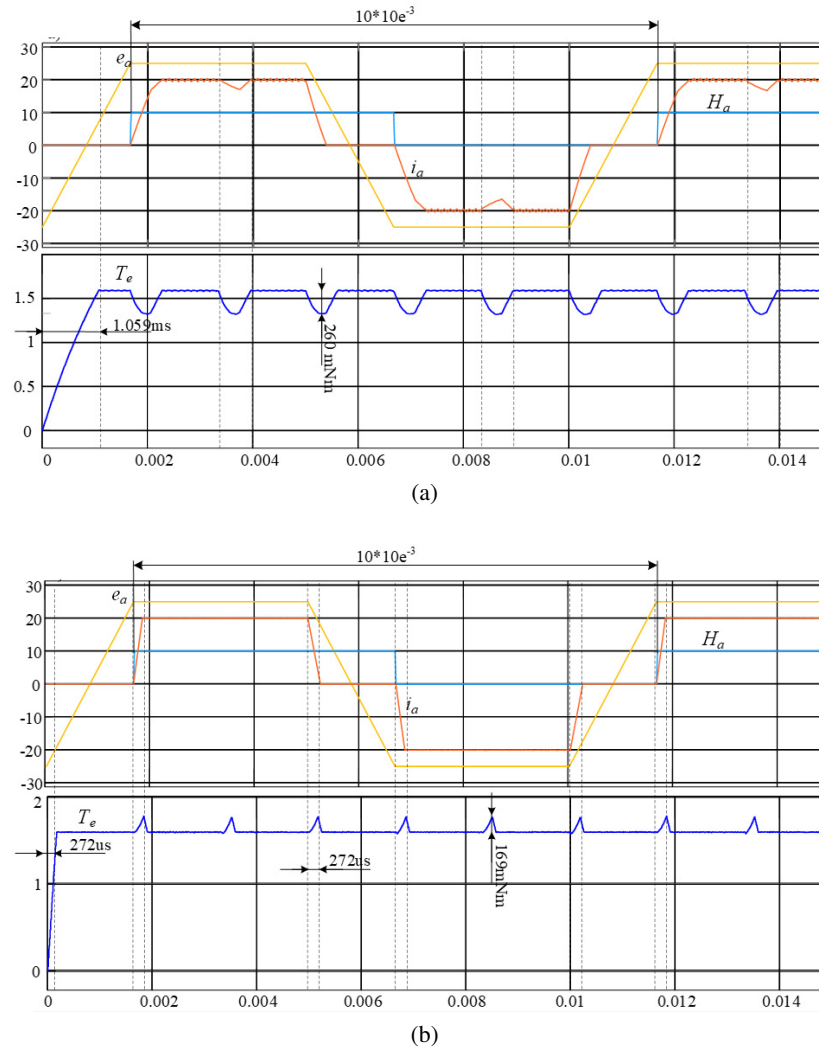
(a)

(b)

Fig. 9. Waveforms of the current of a single motor phase, back EMF, position sensor and electromagnetic torque signal recorded for: (a) the classic unipolar modulation; (b) proposed solution

The comparison of the unipolar modulation and the proposed solution (Fig. 10(a) and Fig. 10(b)) demonstrates that the new solution allows for a significant reduction in the time of current commutation (from 0.4×10^{-3} to 0.24×10^{-3}) and the independent supply of each of the phases prevents the problem of conducting phase current reduction during current commutation in other phases (Fig. 10(a)). Furthermore, Fig. 10 demonstrates a twofold increase in the AC component of the current and twofold reduction in its value (from 1.2 A to 0.6 A). A reduction in the current ripples is achieved thanks to these properties. As Equation (5) shows, a reduction of the AC component of the current causes a reduction in torque ripples.
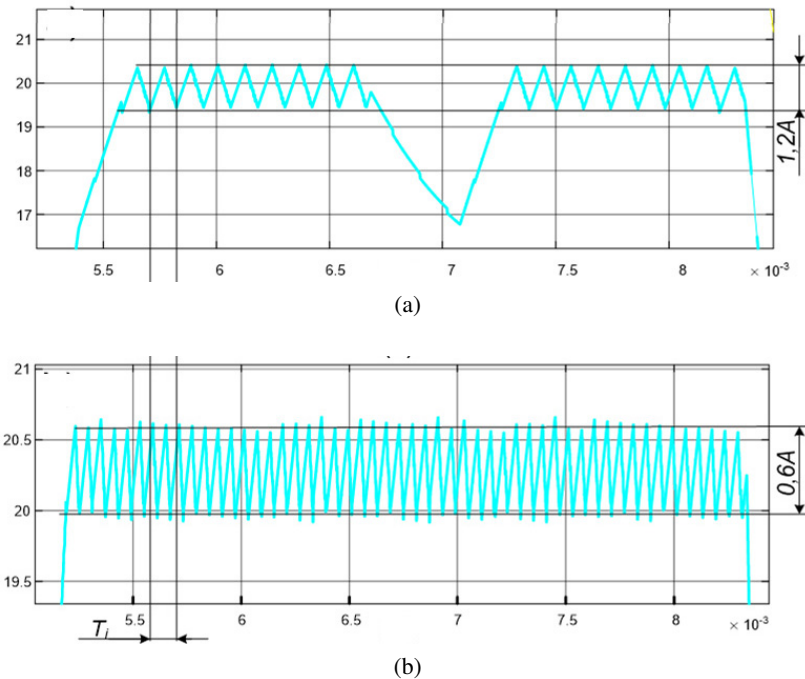
(a)

(b)

Fig. 10. Zoomed in waveforms of the current of a single motor phase developed for: (a) the classic unipolar modulation; (b) proposed solution

The presented analyses demonstrate that the proposed supply method allows for reducing the current ripples (resulting from the switching operation).

6. Experimental setup

After completion of work with the simulator, the algorithm was transferred into a real converter with a power circuit in accordance with the diagram from Fig. 1 and based on IGBT modules SK25GD126ET manufactured by Semicron. The experimental setup was equipped with a high-speed BLDC motor with a rated power of 2 kW. All waveforms presented in this chapter were recorded for velocity 3 991.2 RPM (presented solution) and 1 995.6 RPM (classic unipolar modulation).

The presented considerations have been checked in a real system which made it possible to change the voltage at the dc-link capacitor. The transistor switching frequency has been fixed at 17.1 kHz. Fig. 11(a) presents oscilloscope traces of the current of a motor supplied in accordance with the described solution. Fig. 11(b) presents the same waveforms recorded for the motor connected in star configuration and supplied from a bridge power inverter with unipolar modulation [19, 20].

As it results from comparing the waveforms in Fig. 11, at the same operating conditions (the same dc-link voltage, identical power inverter, the same transistor switching frequency) the motor supplied in accordance with the presented solution has accelerated to a speed two times higher than in the case of the power supply typical for BLDC motors with unipolar modulation. A comparison of the motor current ac component frequency is presented in Fig. 12.

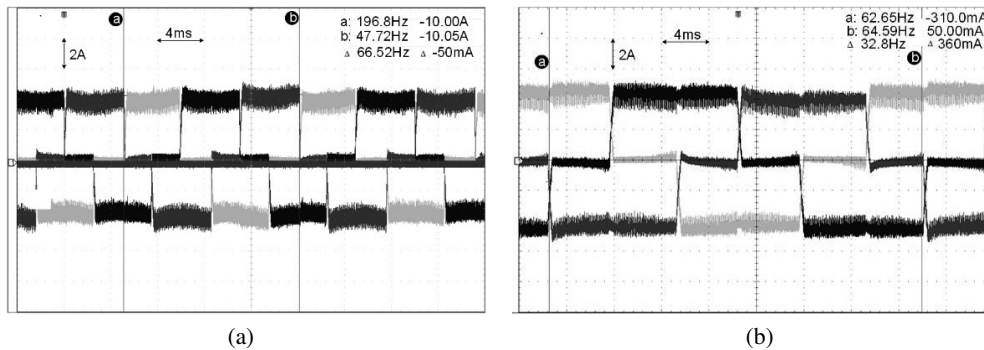(a)   (b)

Fig. 11. Current waveforms for three motor phases recorded for: (a) unassociated motor windings powered as in Fig. 1; (b) windings connected in star configuration and supplied from a typical bridge power inverter

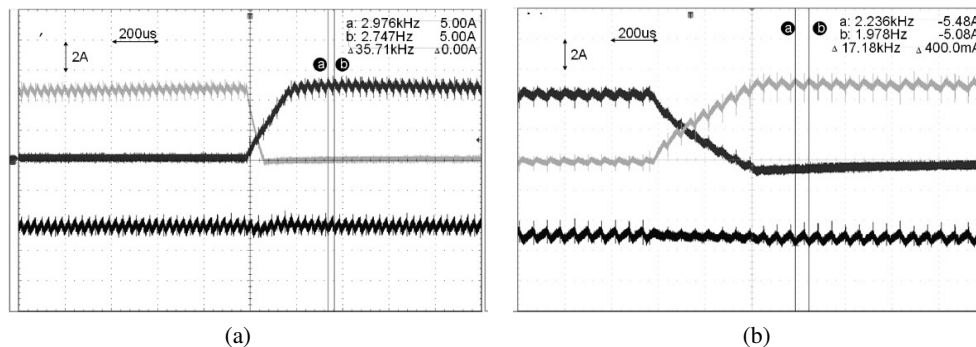(a)   (b)

Fig. 12. Current waveforms for three motor phases with power supply: (a) as in Fig. 1; (b) from a bridge power inverter typical for BLDC motors with unipolar modulation

In BLDC motors, the electromagnetic torque is proportional to the current flowing through the windings. As it results from the comparison presented in Fig. 12, the switching frequency of the sum of currents of a motor supplied as in Fig. 1 is four times higher than the transistor switching frequency. In the case of conventional power supply, however, the switching frequency of the sum of currents is equal to the transistor switching frequency. Besides, the ac component value of the sum of currents in the described solution is four times lower than in the typical power supply method. From this it follows that the value of torque pulsation resulting from the pulsed operation of the power supply system will be four times lower than in the case of suppling the motor with power from a bridge power inverter.

In the described solution, the current ac component frequency (with the same transistor switching frequency) is two times higher (35.71 kHz) than with unipolar modulation in a bridge power inverter (17.18 kHz). From the comparison presented in Fig. 12 it can be read that the process of current switching between successive phases in the described solution is almost two times shorter than with the conventional method of supplying a BLDC motor. The waveforms of the pulses controlling one of the power inverter transistors, the current of two motor phases (i_a, i_b), and the current of the dc-link capacitor (i_{cf}) are presented in Fig. 13.
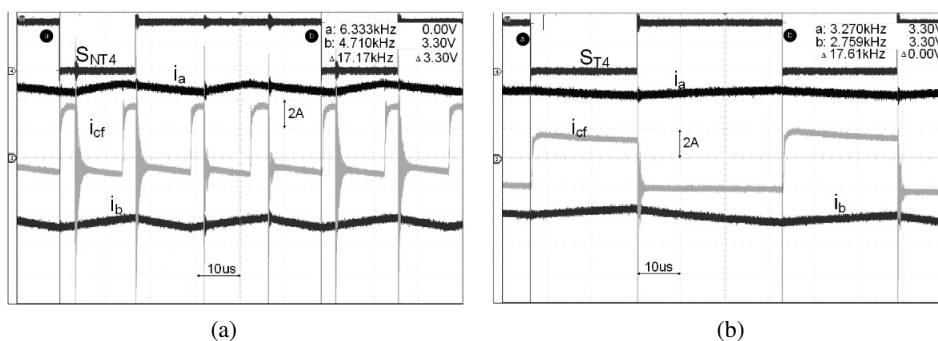

Fig. 13. Waveforms of current for two motor phases, capacitor current (i_{cf}), pulses controlling one of the transistors with power supply: (a) as in Fig. 1; (b) from a bridge power inverter typical for BLDC motors with unipolar modulation

As shown by the waveforms in Fig. 13(a), thanks to the phase shift in transistor control, the AC component of a capacitor current can be obtained four times higher than the transistor switching frequency. Thanks to this feature, the dc-link capacitor can have lower capacity than in typical systems.

Waveforms of the absolute value of two phase currents of the BLDC motor ($|i_a|$, $|i_b|$) and the sum of these values ($|i_a| + |i_b|$), as well as pulses controlling one of the transistors are presented in Fig. 14.
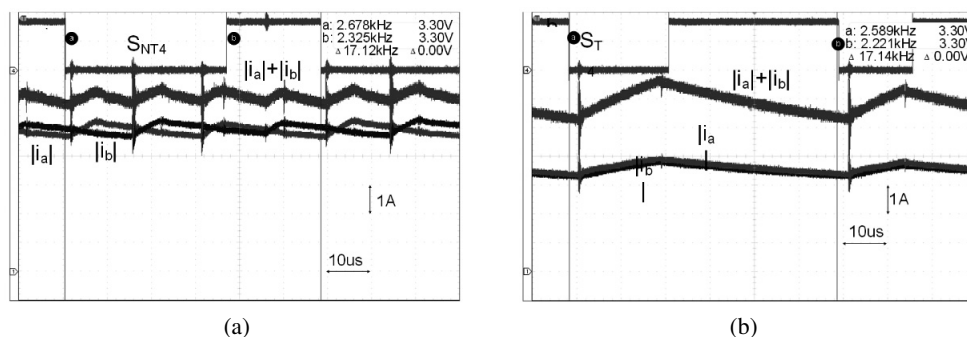

Fig. 14. Waveforms of the absolute value of current for two motor phases, sum of these values, pulses controlling one of the transistors with power supply: (a) as in Fig. 1; (b) from bridge power inverter typical for BLDC motors with unipolar modulation

7. Conclusions

A method for open-end winding BLDC motor power supply has been presented in the paper. The described power supply method has a number of advantages over the conventional method. These advantages have been described in Table 4.

Table 4. Comparison of the described power supply method with supplying a BLDC motor from a bridge power inverter with unipolar modulation

	Windings connected in star configuration, unipolar modulation	**Open-end windings**
Maximum speed possible with the same capacitor voltage	Two times lower than in an open-end winding motor	Two times higher than in a conventionally supplied motor
Phase current ac component frequency	Equal to the transistor switching frequency	Two times higher than the transistor switching frequency
Capacitor current ac component frequency	Equal to the transistor switching frequency	Four times higher than the transistor switching frequency
Current switching between windings	Hindered, takes longer than with open-end winding	There is no problem of taking the current over by successive windings
Torque pulsation resulting from pulsed operation of the power inverter	Pulsation frequency equal to the transistor switching frequency, torque ac component value four times higher than for open-end winding motor	Pulsation frequency four times higher than the transistor switching frequency, torque ac component value four times lower than for conventionally supplied motor
Voltage class of semiconductor elements while maintaining the same rotational speed	At least two times higher than resulting from the BEMF voltage	Greater than the BEMF voltage
Capacitor voltage while maintaining the same rotational speed	At least two times higher than resulting from the BEMF voltage	Greater than the BEMF voltage

References

[1] Dziadecki A., Grzegorski J., Skotniczny J., *Sensorless control system of SRM drive*, Przeglad Elektrotechniczny, vol. 88, no. 8, pp. 317–322 (2012).

[2] Yang Y., Ting Y., *Improved Angular Displacement Estimation Based on Hall-Effect Sensors for Driving a Brushless Permanent-Magnet Motor*, IEEE Transactions on Industrial Electronics, vol. 61, no. 1, pp. 504–511 (2014).

[3] Xia C., Xiao Y., Chen W., Shi T., *Torque Ripple Reduction in Brushless DC Drives Based on Reference Current Optimization Using Integral Variable Structure Control*, IEEE Transactions on Industrial Electronics, vol. 61, no. 2, pp. 738–752 (2014).

[4] Masmoudi M., Badsi B., Masmoudi A., *DTC of B4-Inverter-Fed BLDC Motor Drives With Reduced Torque Ripple During Sector-to-Sector Commutations*, IEEE Transactions on Power Electronics, vol. 29, no. 9, pp. 4855–4865 (2014).

[5] Chun T., Tran Q., Lee H., Kim H., *Sensorless Control of BLDC Motor Drive for an Automotive Fuel Pump Using a Hysteresis Comparator*, IEEE Transactions on Power Electronics, vol. 29, no. 3, pp. 1382–1391 (2014).

[6] Dadashnialehi A., Bab-Hadiashar A., Cao Z., Kapoor A., *Intelligent Sensorless Antilock Braking System for Brushless In-Wheel Electric Vehicles*, IEEE Transactions on Industrial Electronics, vol. 62, no. 3, pp. 1629–1638 (2015).

[7] Tsotoulidis S., Safacas A., *Deployment of an Adaptable Sensorless Commutation Technique on BLDC Motor Drives Exploiting Zero Sequence Voltage*, IEEE Transactions on Industrial Electronics, vol. 62, no. 2, pp. 877–886 (2015).

[8] Cui G., Liu G., Wang K., Song X., *Sensorless Drive for High-Speed Brushless DC Motor Based on the Virtual Neutral Voltage*, IEEE Transactions on Power Electronics, vol. 30, no. 6, pp. 3275–3285 (2015).

[9] Jung S., Kim J., Jae J., Kim J., *Commutation Control for the Low-Commutation Torque Ripple in the Position Sensorless Drive of the Low-Voltage Brushless DC Motor*, IEEE Transactions on Power Electronics, vol. 29, no. 11, pp. 5983–5994 (2014).

[10] Cui C., Liu G., Wang K., *A Novel Drive Method for High-Speed Brushless DC Motor Operating in a Wide Range*, IEEE Transactions on Power Electronics, vol. 30, no. 9, pp. 4998–5008 (2015).

[11] Ciurys M.P., *Analysis of the influence of inverter PWM speed control methods on the operation of a BLDC motor*, Archives of Electrical Engineering, vol. 67, no. 4, pp. 939–953 (2018).

[12] Tokyo Shibaura Electric Co., *Inverter and air conditioner controlled by the same*, U.S. Patent 5 486 743 (1996).

[13] Gui-Jia S., McKeever J.W., *Low-cost sensorless control of brushless DC motors with improved speed range*, IEEE Transactions on Power Electronics, vol. 19, no. 2, pp. 296–302 (2004).

[14] Becerra R.C., Jahns T.M., Ehsani M., *Four-quadrant sensorless brushless ECM drive*, APEC '91: Sixth Annual Applied Power Electronics Conference and Exhibition, Dallas, TX, USA, pp. 202–209 (1991).

[15] Shao J., Nolan D., Teissier M., Swanson D., *A novel microcontroller-based sensorless brushless DC (BLDC) motor drive for automotive fuel pumps*, IEEE Transactions on Industry Applications, vol. 39, no. 6, pp. 1734–1740 (2003).

[16] Lai Y., Shyu F., Chang Y., *Novel loss reduction pulsewidth modulation technique for brushless dc motor drives fed by MOSFET inverter*, IEEE Transactions on Power Electronics, vol. 19, no. 6, pp. 1646–1652 (2004).

[17] Tokyo Shibaura Electric Co., *Drive control apparatus for brushless DC motor and driving method therefore*, U.S. Patent 5 491 393 (1996).

[18] Rajeevan P.P., Sivakumar K., Gopakumar K., Patel C., Abu-Rub H., *A Nine-Level Inverter Topology for Medium-Voltage Induction Motor Drive With Open-End Stator Winding*, IEEE Transactions on Industrial Electronics, vol. 60, no. 9, pp. 3627–3636 (2013).

[19] Wei J., Deng Q., Zhou B., Shi M., Liu Y., *The Control Strategy of Open-Winding Permanent Magnet Starter-Generator With Inverter-Rectifier Topology*, IEEE Transactions on Industrial Informatics, vol. 9, no. 2, pp. 983–991 (2013).

[20] de Almeida Carlos G.A., dos Santos E.C., Jacobina C.B., Mello J.P.R.A., *Dynamic Voltage Restorer Based on Three-Phase Inverters Cascaded Through an Open-End Winding Transformer*, IEEE Transactions on Power Electronics, vol. 31, no. 1, pp.188–199 (2016).

[21] Kim Y., Kyung-Won J., Lee T., Kim Y., Jung S., *Design and control methodology analysis of BLDC motor for torque ripple minimization considering winding connection*, 2013 International Conference on Electrical Machines and Systems (ICEMS), Busan, pp. 1109–1112 (2013).

[22] Qiu J., Shi C., *Sensorless control of brushless DC motor with delta connection windings*, 2010 International Conference on Electrical Machines and Systems, Incheon, pp. 848–851 (2010).

[23] Seol H., Lim J., Kang D., Park J.S., Lee J., *Optimal Design Strategy for Improved Operation of IPM BLDC Motors With Low-Resolution Hall Sensors*, IEEE Transactions on Industrial Electronics, vol. 64, no. 12, pp. 9758–9766 (2017).

[24] Chen S., Sun W., Wang K., Liu G., Zhu L., *Sensorless High-Precision Position Correction Strategy for a 100 kW@20 000 r/min BLDC Motor With Low Stator Inductance*, IEEE Transactions on Industrial Informatics, vol. 14, no. 10, pp. 4288–4299 (2018).